Support Information

Improving thermoelectric performance of Cu_2SnSe_3 via regulating micro- and electronic structures

Hongwei Ming[a,b], Chen Zhu[a,b], Xiaoying Qin[a,*], Bushra Jabar[a,b], Tao Chen[a,b], Jian Zhang[a,*], Hongxing Xin[a,*], Di Li[a], Jinhua Zhang[a,b]

[a]Key Lab of Photovoltaic and Energy Conservation Materials, Institute of Solid State Physics, HFIPS, Chinese Academy of Sciences, Hefei 230031, China.

[b]University of Science and Technology of China, 230026 Hefei, PR China.

[*]Corresponding authors.

Email address: xyqin@issp.ac.cn (X.Y. Qin), zhangjian@issp.ac.cn (J. Zhang), xinhongxing@issp.ac.cn (H. Xin)

1. Experimental and computational procedures

1.1 Sample preparations

Polycrystalline CSS samples were synthesized by melting in vacuum. For this purpose element copper (3N), tin (5N) and selenium (5N) powders (Alfa Aesar) were weighted accurately according to the desired composition, and then sealed in quartz tubes. The vacuum sealed quartz tubes were slowly heated in a furnace to 1193K and kept for 8h, and then the furnace cooled down to 973K and maintained for 48h, followed by cooling to room temperature. The obtained ingot was milled into powders in atmosphere with vibration ball milling for different milling time t_m (t_m =0.5, 1, 1.5, 2, 3h). Finally, in order to obtain bulk samples, the CSS powders of about 2.5g were compacted by hot-pressing at 673K for 1 hour under a pressure of 250MPa.

1.2 Microstructure characterization and property measurements

The phase structure analyses were carried out by using X-ray diffraction (XRD) (model: X'Pert Pro) with Cu K_α radiation (λ=1.5406 Å). The morphologies of the fracture surface were observed by field emission scanning electron microscopy (SEM) (model: SU8020) and high resolution transmission electron microscropy (HRTEM, JEOL-F2010). The electrical conductivity and thermopower of bulk samples were measured from 300K to 848K in a helium atmosphere by using a commercial apparatus (ZEM-3 system, ULVAC-RIKO). Thermal diffusivity α was measured by laser flash method by using a Netzsch LFA 457 instrument, and heat capacity C_p is referred to the Dulong-Petit approximation. The thermal conductivity κ of the samples were obtained by using the relation $\kappa=D\alpha C_p$, with the density D of the bulk samples being determined by Archimedes method. The densities of all investigated samples are in the range of ~5.6-5.7 gcm^{-3} (listed in Table S1), corresponding to the relative density of ~96%. The Hall coefficient (R_H) was determined by the Van der Pauw method; the Hall carrier concentration (p) was calculated from the relations $p=1/(R_H e)$, where e is the electron charge. The positron annihilation lifetime spectra was measured with a 20μCi Na sources and the resolving time is 192ps.

1.3 Computational details

The theoretical results were computed within DFT as implemented in the Vienna ab initio simulation package (VASP[1]) in combination with the projected augmented -wave method[2]. The generalized gradient approximation with Perdew-Burke-Ernzerhof was chosen for determination of exchange correlation energy. Here, a Hubbard-like term +U (U=4eV) was introduced to

correctly describe the localization characteristic of copper's 3d block[3]. A plane-wave cutoff energy of 500eV was set up in which Cu 3d electrons, Se 4s4p electrons and Sn 5s5p electrons were treated as valence electrons. Supercell models of $Cu_{64}Sn_{31}Se_{96}$ and $Cu_{32}Sn_{15}Se_{54}$ were used to calculate the electronic structure of CSS with Sn vacancies. Models of Cu-Sn-terminated-(0 0 -1)-oriented-4-layers-thick crystal slabs of CSS (CSS_{4CS}) and Se-terminated-(0 0 1)-oriented-4-layers-thick crystal slabs of CSS (CSS_{4S}) were built, in which the dangling bonds in the bottom layer were fixed by pseudo H. Besides, a vacuum lay with thickness of 15 Å was used to ensure decoupling between neighbouring slabs. An energy conversion criterion of $1 \times 10^{-5} eV$ per atom were used for the calculation of the density of states and the charge density.

2. Sample density of all investigated samples

Table S1 The sample density (D) and the relative density (D_r)of all investigated samples with different milling time (t_m=0.5, 1, 1.5, 2 and 3h).

Sample	t_m=0.5h	t_m=1h	t_m=1.5h	t_m=2h	t_m=3h
D (g/cm^3)	5.62	5.60	5.64	5.58	5.61
D_r (%)	96.6	96.2	96.9	95.8	96.4

3. Phase and Characterization

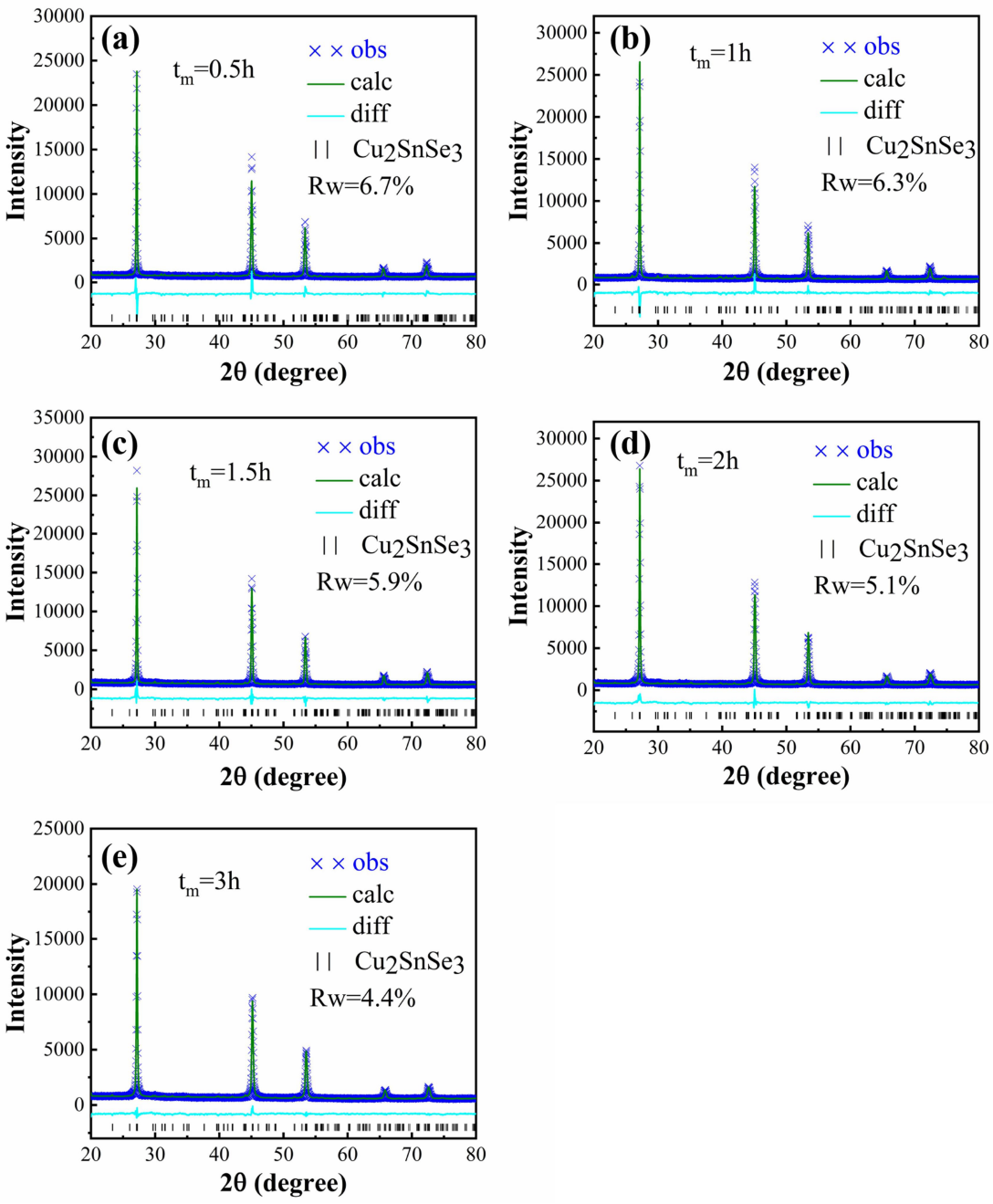

Figure S1 The Rietveld refinement results of Cu_2SnSe_3 samples with milling time t_m=0.5 (a), t_m=1 (b), t_m=1.5 (c), t_m=2 (d) and t_m=3 (e), respectively.

Table S2 The atomic coordinates and site occupancy factor (SOF) of Cu_2SnSe_3 sample with milling time t_m=0.5h.

ATOMS	X	Y	Z	SOF
Cu1	0.3868	0.2450	0.6549	0.9998
Cu2	0.3700	0.4180	0.1160	0.9996
Sn	0.3783	0.0832	0.1182	0.9974
Se1	-0.0172	0.4274	0.0034	1.0005
Se2	-0.0168	0.0899	-0.0159	1.0000
Se3	0.4924	0.2522	-0.0197	1.0000

Table S3 The atomic coordinates and site occupancy factor (SOF) of Cu_2SnSe_3 sample with milling time t_m=1h.

ATOMS	X	Y	Z	SOF
Cu1	0.3710	0.2570	0.6160	0.9997
Cu2	0.3207	0.4083	0.0811	1.0000
Sn	0.3624	0.08940	0.1047	0.9941
Se1	-0.0268	0.4242	-0.0043	1.0000
Se2	-0.0141	0.0861	-0.0085	1.0007
Se3	0.5030	0.2590	-0.0140	1.0002

Table S4 The atomic coordinates and site occupancy factor (SOF) of Cu_2SnSe_3 sample with milling time t_m=1.5h.

ATOMS	X	Y	Z	SOF
Cu1	0.3694	0.2530	0.6243	0.9998
Cu2	0.3717	0.4117	0.1176	1.0000
Sn	0.3571	0.0817	0.1092	0.9897
Se1	-0.0096	0.4199	-0.0104	1.0000
Se2	-0.0033	0.0842	-0.0238	1.0010
Se3	0.4910	0.2546	-0.0029	1.0000

Table S5 The atomic coordinates and site occupancy factor (SOF) of Cu_2SnSe_3 sample with milling time t_m=2h.

ATOMS	X	Y	Z	SOF
Cu1	0.3577	0.2538	0.6141	0.9996
Cu2	0.3525	0.4086	0.0975	0.9978
Sn	0.3619	0.0796	0.1198	0.9823
Se1	-0.0201	0.4175	-0.0041	1.0000
Se2	-0.0079	0.0853	-0.0204	1.0000
Se3	0.4910	0.2507	0.0079	1.0001

Table S6 The atomic coordinates and site occupancy factor (SOF) of Cu_2SnSe_3 sample with milling time t_m=3 hours.

ATOMS	X	Y	Z	SOF
Cu1	0.3655	0.2496	0.6121	0.9992
Cu2	0.3711	0.4098	0.1180	1.0000
Sn	0.3659	0.0861	0.1448	0.9682
Se1	-0.0200	0.4131	-0.0101	1.0000
Se2	-0.0104	0.0879	-0.0171	1.0012
Se3	0.4817	0.2487	-0.0005	0.9985

4. Microstructure characterization with SEM

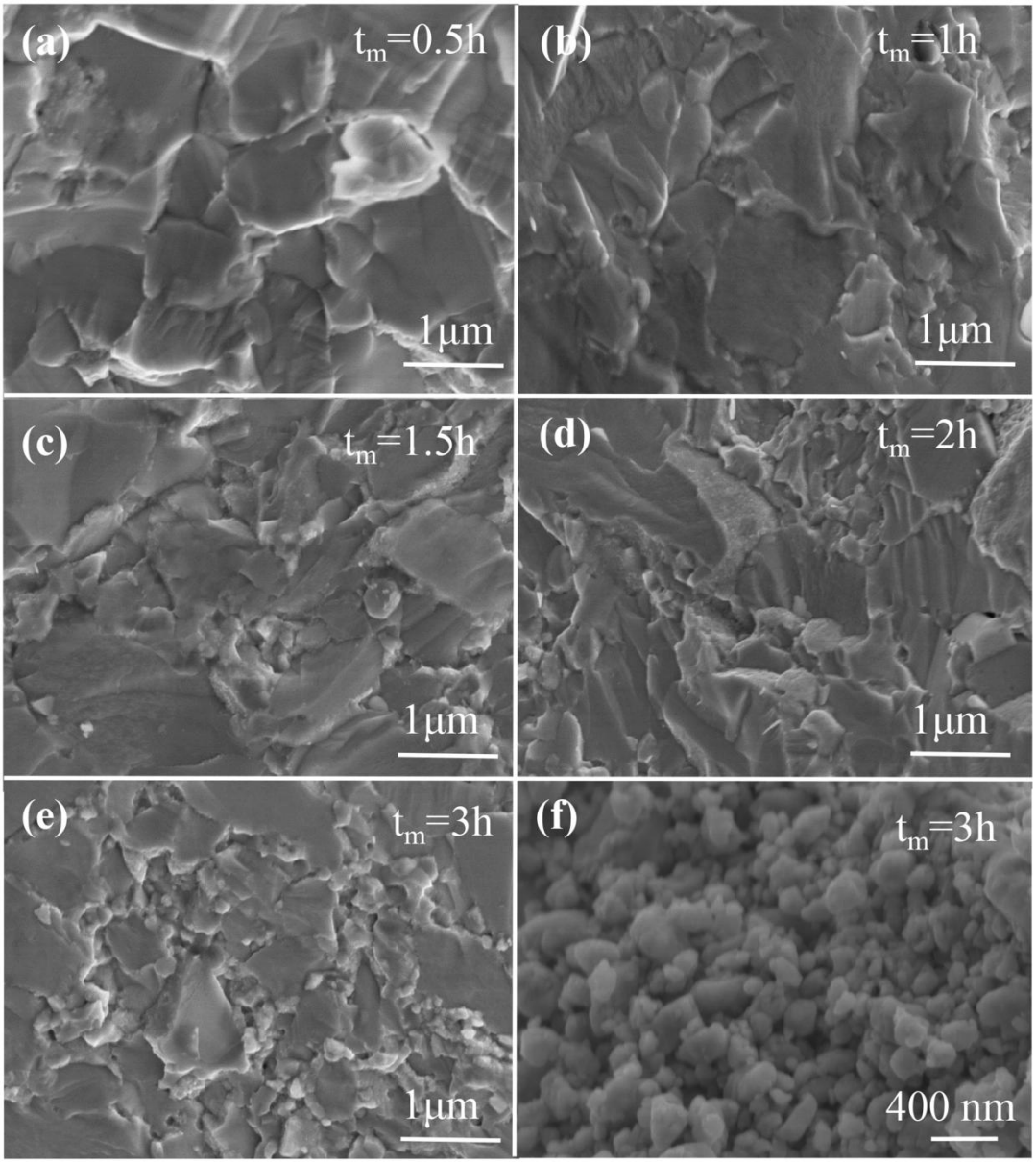

Figure S2. SEM images of the fracture surface of Cu_2SnSe_3 with different milling time, t_m=0.5h (a), t_m=1h (b), t_m=1.5h (c), t_m=2h (d) and t_m=3h (c); (f) the SEM images of the powder of Cu_2SnSe_3 sample that was milled for 3h.

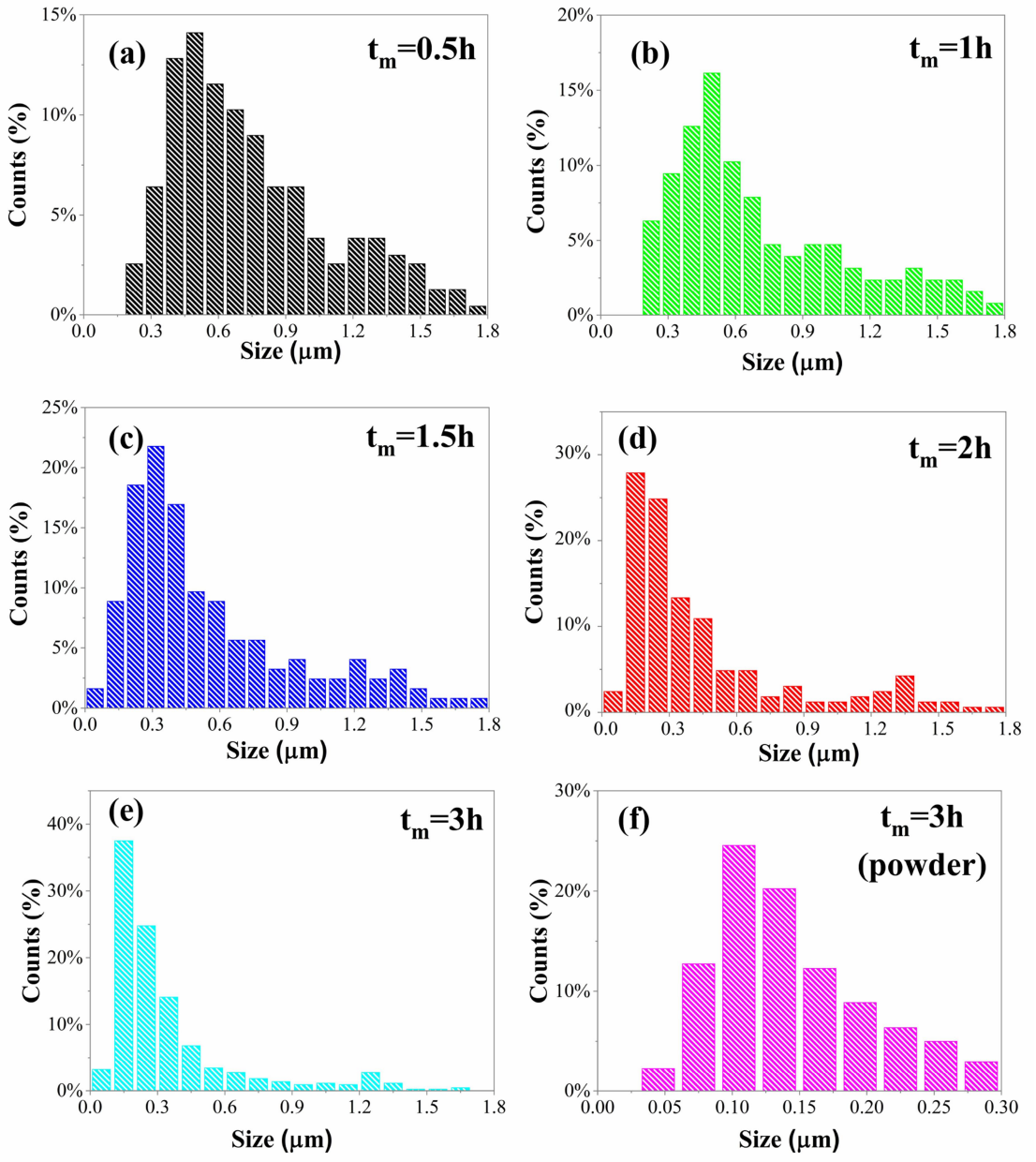

Figure S3. The grain size distribution of the fracture surface of Cu_2SnSe_3 with different milling time, t_m=0.5h (a), t_m=1h (b), t_m=1.5h (c), t_m=2h (d) and t_m=3h (e); (f) the grain size distribution of the powder of Cu_2SnSe_3 sample that was milled for 3h.

5. **Bonding characteristics and the defect states of Cu_2SnSe_3**

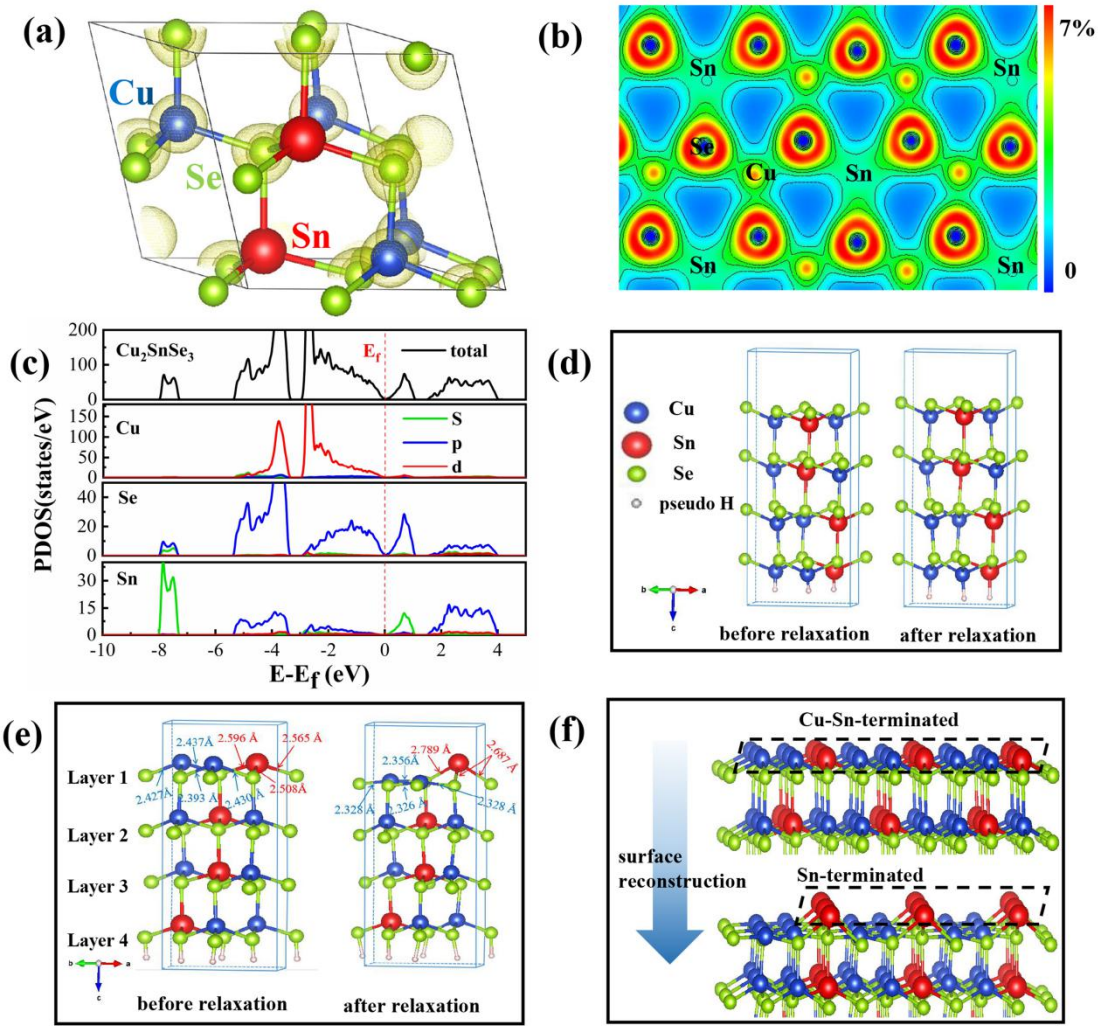

Figure S4. (a) Charge density distribution of Cu_2SnSe_3; (b) contour plots of charge density distribution on (0 0 1) plane; (c) the PDOS of Cu_2SnSe_3; the crystallographic structure of CSS_{4S} (d) and CSS_{4CS} (e), the left is the structure before relaxation and the right one is after relaxation; (f) schematic diagram of the surface reconstruction from Cu-Sn-terminated Cu_2SnSe_3 to Sn-terminated structure.

For better understanding the counter-intuitive formation of SnO_2 in CSS compounds, first principle calculations were performed to analyze the characteristics of Cu-Se and Sn-Se bonds. Figure S4(a)&(b) show the charge density distribution for CSS and the (001) plane, which can display the primary bond network in the material in real space. According to Figure S4(a)&(b), one can see that the charge density accumulates mainly in the line linking Cu and Se atom, which means that Cu-Se bonds play the dominant role in controlling the carrier transport. Besides, the Sn

atoms exhibit little charge density accumulation in the area linking with Se, which means that Sn orbitals just offer electrons to the system and do not contribute much for the hole transport[3]. Analysis on the partial density of states (PDOS) also shows that the strong d-p hybridization from Cu-Se bonds to form strong covalent bonding[3] and contribute to valance band maximum (VBM) (as shown in Figure S4(c)); weak interactions between Sn p and Se p orbitals in the lower valance band to form chemical bonds, but they make negligible contribution to the states near VBM for the carrier transport. In short, Cu-Se bonds stabilize the structure and form an electrically conductive framework by the strong covalent bonding, and Sn atoms reside in the framework to balance the structure and donate electrons for the weak Sn-Se interaction[3]. Figure S4(d)&(e) show the crystallographic structure of Se-terminated-(0 0 1)-oriented-4-layers-thick crystal slabs of CSS (CSS_{4S}) and Cu-Sn-terminated-(0 0 -1)-oriented-4-layers-thick crystal slabs of CSS (CSS_{4CS}). We can see from Figure S4(d) that the there is little change of the structure of CSS_{4S} after relaxation, which means that the Se-terminated CSS is stable. However, significant surface reconstruction can be observed for CSS_{4CS} after relaxation, as shown in Figure S4(e). Specifically, after relaxation the Cu-Se bonds become shorter than that of the unrelaxed one and the Sn-Se bonds become longer than before, which means the stronger Cu-Se bonds and the weaker Sn-Se interaction. One can see from Figure S4(f) that after surface reconstruction, the Sn atoms were moved out of the Cu/Sn plane, which explains why Sn vacancy and SnO_2 form and no copper oxides being observed in our experiments.

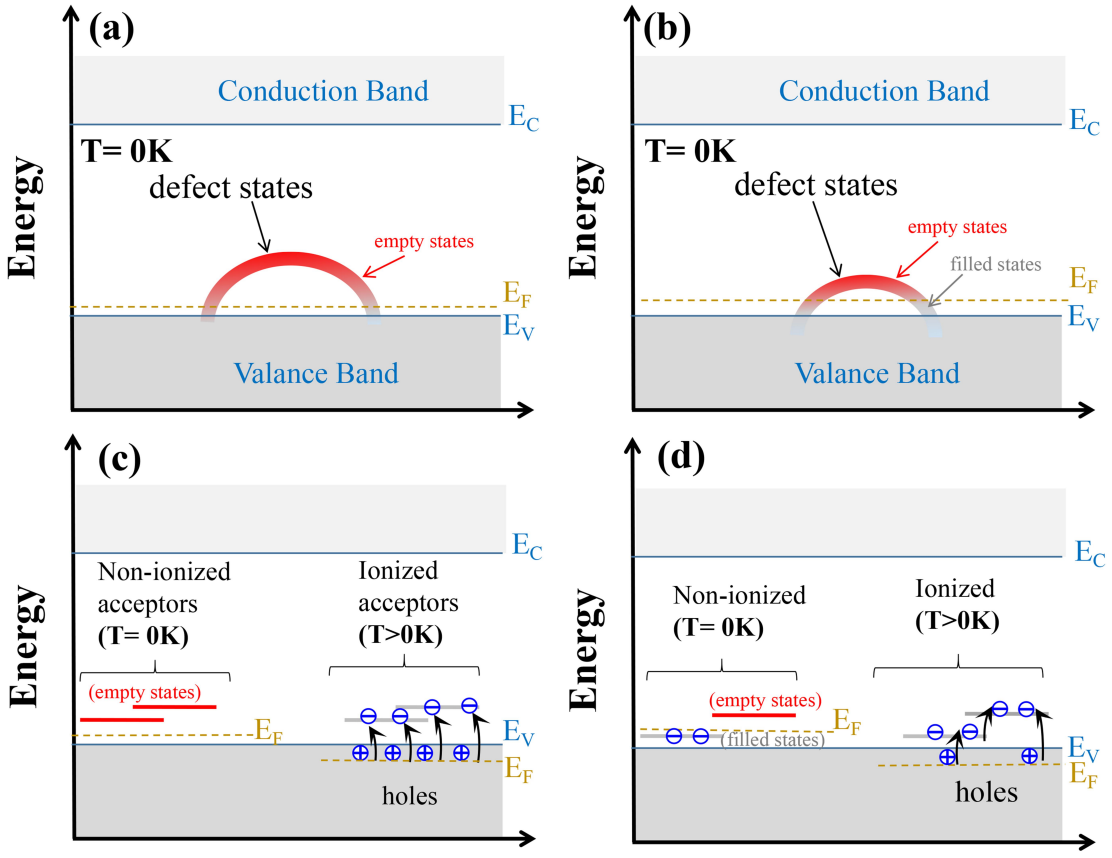

Figure S5. Energy-band diagram showing the defect states caused by Se dangling bonds (a) and Cu/Sn surface reconstruction (b); the schematic that show how defect state contribute holes to host valence band (c)&(d).

Figure S5(a) shows the energy-band diagram of the defect states caused by the Se dangling bonds. These defect states can be simplified as many discrete acceptor levels shown in Figure S5(c). One can see that at 0 K electrons fill up the valance bands, as the temperature rises above 0 K, the electron in the valance bands will be excited to the shallow acceptor level and donate hole carriers to the host (valence band). Figure S5(b) shows the defect states caused by the reconstruction of Cu/Sn-terminated surface. One can see from Figure S5(b) that, at 0K the defect states are partially filled with electrons and partially empty, therefore, the discrete energy levels can be simplified as Figure S5(d). At 0 K the defect levels are partially filled with electrons and partially empty, as T rises above 0K the electron in the valance bands will be excited to the empty energy levels, which will donate hole carriers to the host (valence band); and/or the electron in the filled defect energy level will be excited to the empty defect levels of higher, leaving empty acceptor energy levels with lower energies, which can also trap the electrons excited form the valance band.

6. The temperature dependence of thermal conductivity from carriers (holes)

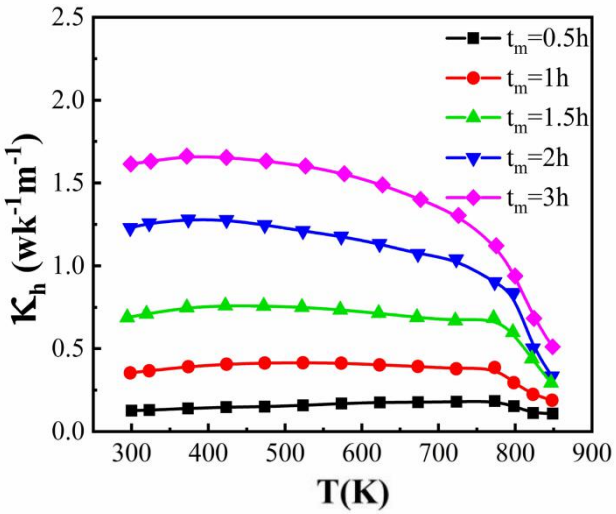

Figure S6. Temperature dependence of the thermal conductivity from holes κ_h for CSS sample with different milling time (t_m=0.5, 1, 1.5, 2 and 3h), where κ_h=LσT, and the Lorenz number L= $1.5+\exp(-|S|/116)\times 10^{-8}V^2K^{-2}$.

7. Obtained parameters in Debye-Callaway model

Table S7. The parameters A, B, C and D used in Debye-Callaway model and the experimentally determined grain size *l* .

t_m (hour)	A ($10^{-42}s^3$)	B (10^{-17}s/K)	C (10^{-3})	D ($10^{-29}s^2$)	*l* (nm)
0.5	0.18	1.36	0	0	683
1	0.35	1.40	3	1.2	568
1.5	1.06	1.79	3.4	2.5	416
2	1.47	1.90	5.9	3.3	296
3	1.87	2.98	9.5	8.5	240

8. Calculation details of Debye temperature θ_D and average sound velocity V_S

The elastic stiffness constant C_{ij} of Cu_2SnSe_3 was calculated in VASP. According to the transformation of coordinates, the C_{ij} of Cu_2SnSe_3 was given as following:

$$C_{ij} = \begin{pmatrix} 99.44 & 42.27 & 51.12 & 0 & -7.72 & 0 \\ 42.27 & 101.00 & 44.49 & 0 & 1.17 & 0 \\ 51.12 & 44.49 & 100.74 & 0 & 7.80 & 0 \\ 0 & 0 & 0 & 16.76 & 0 & -8.14 \\ -7.72 & 1.17 & 7.80 & 0 & 17.32 & 0 \\ 0 & 0 & 0 & -8.14 & & 27.82 \end{pmatrix}$$

In the monoclinic phase[4],

$B_v = (1/9)\,[C_{11} + C_{22} + C_{33} + 2(C_{12} + C_{13} + C_{23})]$,

$G_v = (1/15)\,[C_{11} + C_{22} + C_{33} + 3(C_{44} + C_{55} + C_{66}) - (C_{12} + C_{13} + C_{23})]$

$B_R = \Omega[a(C_{11} + C_{22} - 2C_{12}) + b(2C_{12} - 2C_{11} - C_{23})]$

$+ c(C_{15} - 2C_{25}) + d(2C_{12} + 2C_{23} - C_{13} - 2C_{22})$

$+ 2e(C_{25} - C_{15}) + f]^{-1}$,

$G_R = 15\{4[a(C_{11} + C_{22} + C_{12}) + b(C_{11} - C_{12} - C_{23}) + c(C_{15} + C_{25}) + d(C_{22} - C_{12} - C_{23} - C_{13}) + e(C_{15} - C_{25})$

$+ f]/\,\Omega + 3[g/\Omega + (C_{44} + C_{66})/\,(C_{44}\,C_{66} - C_{46}^2)]\}^{-1}$,

$a = C_{33}C_{55} - C_{35}^2$,

$b = C_{23}C_{55} - C_{25}C_{35}$,

$c = C_{13}C_{35} - C_{15}C_{33}$,

$d = C_{13}C_{55} - C_{15}C_{35}$,

$e = C_{13}C_{25} - C_{15}C_{23}$,

$f = C_{11}(C_{22}C_{55} - C_{25}^2) - C_{12}(C_{12}C_{55} - C_{15}C_{25}) + C_{15}(C_{12}C_{25} - C_{15}C_{22}) + C_{25}(C_{23}C_{35} - C_{25}C_{33})$,

$g = C_{11}C_{22}C_{33} - C_{11}C_{23}^2 - C_{22}C_{13}^2 - C_{33}C_{12}^2 + 2C_{12}C_{13}C_{23}$,

$\Omega = 2[C_{15}C_{25}(C_{33}C_{12} - C_{13}C_{23}) + C_{15}C_{35}(C_{22}C_{13} - C_{12}C_{23}) + C_{25}C_{35}(C_{11}C_{23} - C_{12}C_{13})] - [C_{15}^2(C_{22}C_{33} - C_{23}^2) + C_{25}^2(C_{11}C_{33} - C_{13}^2) + C_{35}^2(C_{11}C_{22} - C_{12}^2)] + gC_{55}$.

In terms of the Voigt-Reuss-Hill approximations, the bulk modulus B and shear modulus G can be obtained according to the equation as following[4]:

$B = (B_V + B_R)/2$, $G = (G_V + G_R)/2$.

The average sound velocity V_S can be obtained via the following formula[5,6]:

$$V_L = \sqrt{(B + \frac{4G}{3})/\rho}\ ,\ V_T = \sqrt{G/\rho}\ ,\ V_S = \left[\frac{1}{3}\left(\frac{1}{V_L^3} + \frac{2}{V_T^3}\right)\right]^{-1/3}$$

In which ρ is the density, V_L is the longitudinal sound velocity, V_T is the transverse sound velocity. The Debye temperature θ_D can be obtained via $\theta_D = \frac{h}{K_B}\left[\frac{3n}{4\pi}\left(\frac{N_A\rho}{M}\right)\right]^{1/3} V_S$, in which h and K_B is Planck and Boltamann constant, respectively; N_A is the Avogadro's number, n is the number of atoms in the molecule, M is the molecular weight.

9. Thermal stability of thermoelectric properties for Cu_2SnSe_3 sample with t_m=2h

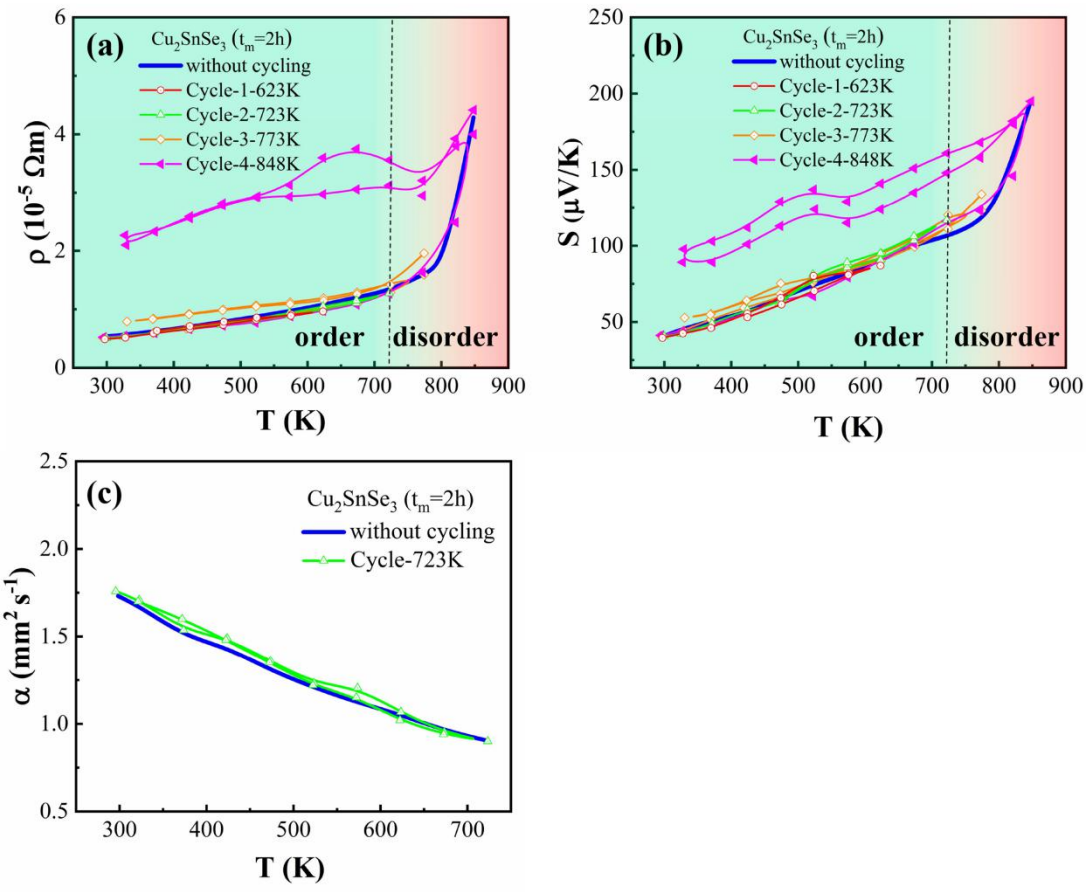

Figure S7. Cycling measurement results of the temperature dependent of electrical resistivity (a), thermopower (b) and thermal diffusivity (c).

References

(1) Kresse, G.; Furthmuller, J. Efficient Iterative Schemes for Ab Initio Total-Energy Calculations Using a Plane-Wave Basis Set. *Phys. Rev. B* **1996**, *54*, 11169-11186.

(2) Kresse, G.; Joubert, D. From Ultrasoft Pseudopotentials to the Projector Augmented-Wave Method. *Phys. Rev. B* **1999**, *59*, 1758-1775.

(3) Xi, L.; Zhang, Y. B.; Shi, X. Y.; Yang, J.; Shi, X.; Chen, L. D.; Zhang, W.; Yang, J.; Singh, D. J. Chemical Bonding, Conductive Network, and Thermoelectric Performance of the Ternary Semiconductors Cu2snx3(X=Se, S) from First Principles. *Phys. Rev. B* **2012**, 86.

(4) Wu Z. J.; Zhao E. J.; Xiaong H. P.; Hao X. F.; Liu X. J.; and Meng J. Crystal Structures and Elastic Properties of Superhard IrN2 and IrN3 from First Principles. *Phys. Rev. B* **2007**, *76,* 054115.

(5) Anderson O. L. A Simplified Method for Calculating the Debye Temperature from Elastic Constants. *J. Phys. Chem. Solids* **1963**, *24*, 909.

(6) Sanditov D. S.; Belomestnykh V. N. Relation between the Parameters of the Elasticity Theory and Averaged Bulk Modulus of Solids. *J. Phys. Chem. Solids* **1959**, *12*, 41.